ACS Sustainable Chemistry & Engineering

Research Article

Cite This: ACS Sustainable Chem. Eng. 2018, 6, 1872−1880

pubs.acs.org/journal/ascecg

Semiconductor Photocatalysis of Bicarbonate to Solar Fuels: Formate Production from Copper(I) Oxide

Hanqing Pan,[†] Sanchari Chowdhury,[‡] Dumindu Premachandra,[†] Sam Olguin,[†] and Michael D. Heagy*[,†]

[†]Department of Chemistry, and [‡]Department of Chemical Engineering, New Mexico Institute of Mining and Technology, 801 Leroy Place, Socorro, New Mexico 87801, United States

Supporting Information

ABSTRACT: Copper-oxide-based photocatalysts, micron- and nanosized, and silver nanoparticle−copper oxide nanocomposites (Ag/Cu_2O) were characterized and evaluated for the first time in the application of bicarbonate conversion to formate. The Ag/Cu_2O nanocomposite yielded considerable production improvement over pure copper oxides due to the role of silver as a plasmonic sensitizer. We attribute these marked production improvements to plasmon-induced electron transfer from metal to semiconductor. These photocatalysts were studied in two different hole scavenger solvents (2-propanol and glycerol) using a solar simulator with air mass coefficient 1.5 and 0 (AM 1.5, AM 0) filters. Formate production increased significantly with AM 0 solar irradiation due to inclusion of the ultraviolet portion of the solar spectrum, and nanoparticulate Cu_2O showed improved photocatalysis relative to micron Cu_2O. Green chemistry solvent, glycerol, proved to be a far superior hole scavenger in comparison to 2-propanol.

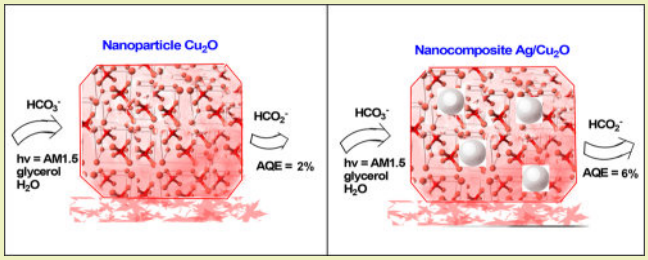

KEYWORDS: *solar fuels, formate, silver nanoparticles, plasmonic sensitizer*

INTRODUCTION

Despite growing public awareness, concentrations of anthropogenic carbon dioxide (CO_2) continue to increase unabated. As the most abundant greenhouse gas, efforts to mitigate this trend have focused on conversion of CO_2 to value-added chemicals or automotive fuels such as formate or methanol, respectively.[1−3] Ideally, CO_2 is photochemically converted without the use of additional CO_2-generating power sources via solar energy. "Photons to formate"[4] presents an economical strategy toward converting this waste gas to a value-added product such as formate, which is a key intermediate toward methanol, a high-octane fuel. The concept of the "methanol economy", championed by Chemistry Nobel laureate George Olah, has been highlighted as an alternative to compressed or adsorbed hydrogen since methanol has a higher energy density than hydrogen, and is renewable, readily transportable, and compatible with our existing infrastructure.[5]

A number of metal oxides and sulfides have been previously reported as semiconductor photocatalysts for CO_2 reduction. For sulfides, ZnS and CdS are the two most widely studied sulfides. ZnS (E_g = 3.87 eV)[6] has been utilized because of its strongly reductive conduction band (E_{CB} = −1.85 V versus NHE), which lies above the lowest unoccupied molecular orbital (LUMO) energy value of CO_2 at −0.61 eV. Due to the efficient electron transfer from E_{CB} of ZnS to the LUMO of CO_2, ZnS has been reported to successfully reduce CO_2 to formate.[7] Henglein[8] and Yoneyama[9] were among the first to study micron-sized ZnS particles, and to study the size effect and other factors that influence photocatalysis rate. Both hypothesized that smaller ZnS particles will be more efficient due to their larger band gap and higher surface area. The hypothesis regarding improved production yields correlating to higher surface area was later confirmed by our group, where the photocatalytic differences of sphalerite and wurtzite were compared via size, crystal structure, surface area, and band gap of ZnS for the reduction of bicarbonate. This work resulted in the highest quantum yield of 3.2%.[10] Other studies involving ZnS to produce formic acid, formaldehyde, and methanol resulted in quantum yields of 0.02%,[11] 0.24%,[12] and 32%.[13] Though incredibly high, the last quantum efficiency was determined at 280 nm, a high-intensity monochromatic wavelength that can significantly boost product yield. Kuwabata and colleagues applied microcrystalline ZnS in the presence of methanol dehydrogenase to reduce CO_2 directly to methanol.[14]

Though there are only a handful of sulfides studied, oxides have been more widely used in CO_2 reduction, and these include TiO_2, WO_3, $SrTiO_3$, $BaTiO_3$, $K_2Ti_6O_{16}$, $InTaO_4$, Zn_2GeO_4, and Ga_2O_3. TiO_2 (P-25, Evonik) is the most widely known and used semiconductor for CO_2 reduction, and its efficiency can be increased by a positive hole scavenger such as isopropyl alcohol.[15−17] Previous studies and reviews discussing CO_2 reduction with Cu_2O or copper-oxide-derived species[18,19]

Received: September 12, 2017
Revised: November 30, 2017
Published: December 6, 2017

DOI: 10.1021/acssuschemeng.7b03244
ACS Sustainable Chem. Eng. 2018, 6, 1872−1880

include photocatalytic,[20−22] electrochemical,[23−26] and photoelectrochemical methods.[27−29] Recently, Lee et al. reported a Ag−Cu_2O electrode to reduce CO_2 to ethanol.[30] The addition of Ag into Cu_2O suppressed hydrogen evolution, thus enhancing the product selectivity toward ethanol. Given these successful catalytic applications involving copper(I) oxide and because the conduction band (CB) of Cu_2O is comparable in energy to the LUMO of bicarbonate, this Earth-abundant, nontoxic material appears appropriate for bicarbonate reduction.[31]

In seeking to optimize copper(I) oxide as a photocatalyst, we also considered that the noble metal nanoparticles of Ag, Au, and Pt have been implemented as plasmonic sensitizers for semiconductors in plasmonic photocatalysis.[32−34] Plasmonic photocatalysis makes use of the fact that metallic nanoparticles exhibit strong features in their extinction spectra in the visible range.[35] This phenomenon, termed surface plasmon resonance (SPR), occurs when the incident radiation of a particular region of wavelengths resonates with the collective oscillations of the electrons in the nanoparticle.[36] This excitation results in energetic electrons on the surface of the nanoparticle that drive photocatalytic transformations.[37] When nanoparticles are in contact with a semiconductor, a Schottky barrier can form that leads to prolonged charge separation, and can also boost the generation of electrons and holes in semiconductors.[38] Recently, Ag-loaded TiO_2 nanocomposites demonstrated better photocatalytic conversion of CO_2 to methanol than pure titanium oxide due to the synergistic effect between UV light excitation and SPR.[39] Therefore, another strategy to enhance semiconductor photocatalysis involves construction of a hybrid particle consisting of metal and semiconductor (Ag/Cu_2O). The advantages of using a hybrid system include maximized metal−semiconductor interaction, as opposed to semiconductors doped with nanoparticles.[40] We hypothesized that such features would facilitate plasmon-induced electron transfer from metal to Cu_2O semiconductor.

This study will present the first of its kind by using Cu_2O as a semiconductor photocatalyst for formate production. The parameters of our investigation include copper(I) oxide size and the effects of silver nanoparticles toward catalytic efficiency. We will also demonstrate how the Ag/Cu_2O hybrid particle acts to significantly increase formate production through plasmon-induced electron transfer from noble metal to the semiconductor. Perhaps overlooked as an emerging and novel photocatalyst for bicarbonate reduction, Cu_2O is brought to light by this report as a material with the highest quantum efficiency compared to studies mentioned above. With apparent quantum efficiencies of formate production for nanoparticulate Cu_2O and Ag/Cu_2O at 1.8% and 5.5%, respectively, under ambient solar conditions, these yields rank among the highest relative to those of other semiconductor photocatalysts.

EXPERIMENTAL SECTION

Materials. Polyvinylpyrrolidone (PVP; MW 40 000), micron and nano copper(I) oxide (Cu_2O), sodium citrate (TSC), silver nitrate ($AgNO_3$), sodium borohydride ($NaBH_4$), ascorbic acid, 2-propanol, glycerol, sodium bicarbonate ($NaHCO_3$), copper(II) chloride ($CuCl_2$), sodium dodecyl sulfate (SDS), sodium hydroxide (NaOH), hydroxylamine hydrochloride ($NH_2OH{\cdot}HCl$) were all purchased from Sigma-Aldrich and used without further purification.

Synthesis of PVP-Coated Silver Nanoparticles.[41] *Preparation of the Silver Seeds.* A 20 mL volume of aqueous solution containing $AgNO_3$ (2.9×10^{-4} M) and TSC (2.5×10^{-4} M) was prepared and cooled in an ice-bath. To this mixture was added an aqueous solution of $NaBH_4$ (0.1 M, 0.6 mL) dropwise with vigorous stirring. The solution became bright yellow immediately. The seeds were then stored in the dark and aged for 2 h prior to use.

Growth of Silver Nanoplates from the Seed Solution. Aqueous PVP (1 wt %, 10 mL), seed solution (100 μL), TSC (2.5×10^{-2} M, 300 μL), and ascorbic acid (0.1 M, 50 μL) were combined. To this solution was added $AgNO_3$ (0.01 M, 5×50 μL) slowly with vigorous stirring. A color change from colorless to yellow, red, and finally green was observed. Then, 1 min after the last addition of $AgNO_3$, the sol was centrifuged at 10 000 rpm for 30 min. The supernatant was removed, and the precipitates were redispersed in Millipore-purified water.

Synthesis of Ag/Cu_2O Nanocomposites.[40] *Synthesis of AgNP.* The Ag NPs with an average size of 5 nm were prepared by sodium citrate reducing $AgNO_3$ aqueous solution. A 150 mL portion of 1 mM AgNO3 was heated to the boiling point, and then 10 mL of 1 wt % sodium citrate was quickly added. The mixture was then kept at boiling for 0.5 h, yielding the gray yellow Ag NPs.

Synthesis of Ag/Cu_2O Nanocomposites. A 1.0 mL portion of as-prepared 1 mM AgNP solution was added into 5 mL of Cu^{2+} solution containing 0.1 M CuCl2 and 0.0338 M sodium dodecyl sulfate (SDS) with shaking. Next, 0.15 mL of 1 M NaOH and 0.25 mL of 0.2 M NH2OH·HCl were added with shaking for 10 s. The mixture was aged for 2 h and centrifuged to separate the nanocomposites. Varying amounts of AgNP (0.2−3 mL) were added to test for differences in catalytic efficiency.

Semiconductor Characterization. *UV−Vis Spectroscopy.* UV−vis spectra of the particles were obtained using a Varian Cary 50 Scan UV−vis spectrophotometer, with wavelength ranging from 800 to 200 nm. Cu_2O samples were dispersed in ethanol, while the AgNP and Ag/Cu_2O samples were dispersed in Milli-Q water.

Size, Crystal Structure, and Surface Area Determination. Dynamic light scattering (DLS) was performed using a Microtrac Zetatrac particle size analyzer to obtain the hydrodynamic radius of the particles. Crystal structure information was obtained using an X'Pert Pro X-ray diffraction (XRD) instrument. BET surface area measurements were performed on a Micromeritics ASAP 2020 surface area and porosity analyzer, and scanning electron microscopy (SEM) was performed using a Hitachi S-4100 scanning electron microscope. Transmission electron microscopy (TEM) and high-Resolution transmission electron microscopy (HR-TEM) were performed using a JEOL-2010 TEM and JEOL-2010F field emission electron microscope.

Diffuse Reflectance Spectroscopy (DRS). The dry Cu_2O powders were analyzed by a Thermo Scientific Evolution 260 Bio UV−vis spectrophotometer with an integrated sphere in order to obtain its band gap. For preparation of the sample, 5% of Cu_2O and 95% KBr pellets were mixed and ground using a mortar and pestle. Wavelengths were scanned from 800 to 200 nm. The resulting absorbance spectra were treated to a Kubelka−Munk function plotted against the energy of the incident light to obtain band gap information.

Cyclic Voltammetry. In order to place the band gaps obtained via DRS on an absolute energy scale, cyclic voltammetry was performed using an EDAQ ET014 Echem electrode kit with a Ag/AgCl reference electrode, platinum wire counter electrode, and a glassy carbon working electrode. The voltage was swept from −1000 to 1000 mV at a rate of 100 mV/s. The electrolyte used was 0.1 M tetraethylammonium tetrafluoroborate ($TBABF_4$) solution in dry acetonitrile. The procedure for CV was adapted from Fang et al.[42] For powder samples, suspensions were made of 1 mg/mL in ethanol and sonicated for 1 h to ensure suspension. After sonication, 60 μL of 5% Nafion solution was added to the suspension, and 4.5 μL of the resulting solution was pipetted onto a glassy carbon electrode (GCE) and allowed to dry. Several applications of the solution were required to ensure full coverage of the GCE surface.[10]

Ion Chromatography. Ion chromatography was performed on a Dionex AS50 IC with a Dionex IonPac ICE-AS6 ion exclusion column and a Thermo Scientific Dionex AMMS-ICE 300 suppressor. The IC instrument is equipped with a Dionex CD25 conductivity detector. Reagents used were 0.4 mM heptafluorobutyric acid as the eluent at a

DOI: 10.1021/acssuschemeng.7b03244
ACS Sustainable Chem. Eng. 2018, 6, 1872−1880

flow rate of 1.2 mL/min and 5 mM tetrabutylammonium hydroxide as the regenerant.

Photoexperiments. The reaction matrix was as follows: a buffer made of 0.3 M $NaHCO_3$, 2 M hole scavenger (2-propanol or glycerol), and Milli-Q water. Cu_2O catalysts were added at an optimized concentration of 1 mg/mL. For catalysts in the solution phase (nanoparticulate Cu_2O and Ag/Cu_2O), 0.5 mL of the catalyst was added. To find the optimal catalyst concentration and optimal rate, the catalyst was first varied from 0.01 to 3 mg/mL as described by Kisch.[43] The optimal catalyst concentration was found to be 1 mg/mL as the rate plateaued with increasing catalyst concentration as seen in the Supporting Information, Figure S1. The matrix was transferred in a quartz tube, sealed, and placed under an ABET Technologies SunLite solar simulator with AM 1.5 (or AM 0) filter for 8 h. The light source was a 1000 W xenon arc lamp with an output of 1000 W/m^2, the equivalent of 1 sun.[44] A light source providing select wavelengths of 365, 400, 525, and 660 nm was custom-built using a Mouser Electronics LED with fwhm of 15 nm, with the same output intensity as the solar simulator. Aliquots were collected at 2 h increments, and formate concentration was quantified by ion chromatography.

Apparent Quantum Efficiency (AQE). Using an Ophir Photonics Nova II laser energy meter, the energy output of the solar simulator was measured. This power measurement was converted to moles of photons per second. This photon flux was then used to calculate the apparent quantum efficiency (AQE) of the catalyst using eqs 1 and 2.

$$n \text{ mol photons} \frac{1 \text{ mol } e^-}{\text{mol photons}} \frac{\text{mol formate}}{2 \text{ mol } e^-} = \text{theoretical} \quad (1)$$

$$\frac{\text{actual mol formate}}{\text{theoretical mol formate}} 100 = \%\text{AQE} \quad (2)$$

RESULTS AND DISCUSSION

XRD spectroscopy (Supporting Information, Figure S2) shows that both micron and nano Cu_2O have a cubic structure (Table 3). DLS confirms that the particles are fairly monodispersed (Supporting Information, Figure S3), and SEM indicates that the Cu_2O particles are aggregated (Figure 1, top) because

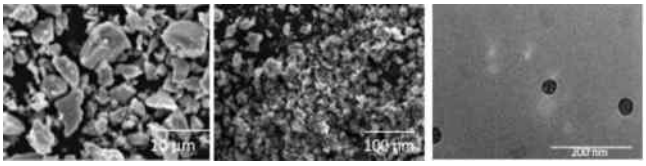

Figure 1. SEM image of (a) micron Cu_2O, and (b) nano Cu_2O. (c) TEM images of nano Cu_2O and Ag/Cu_2O.

nanoparticles are more likely to aggregate in the solution phase.[45] BET surface area measurements (Table 3) showed that nanoparticulates have more surface area than micron-sized particles, as expected for nanoparticles because of their high surface atom to volume ratio.[46] TEM of nanoparticulate Cu_2O (Figure 1) shows that the average size of nano Cu_2O is 30 nm. HR-TEM (Figure 2) further confirms the morphology and composition of the catalysts, showing that in Ag/Cu_2O there are 5 nm silver nanoparticles embedded in Cu_2O. The composition of Ag/Cu_2O was further confirmed by energy dispersive X-ray spectroscopy (EDS; Supporting Information, Figure S4).

UV–vis spectra of Cu_2O taken in the aqueous phase (Supporting Information, Figure S5) do not show any strong absorption. Absorbance spectra are much more prominent when using DRS (Figure 3). Silver nanoparticles (AgNPs) display a plasmon band at 425 nm which is also apparent in Ag/

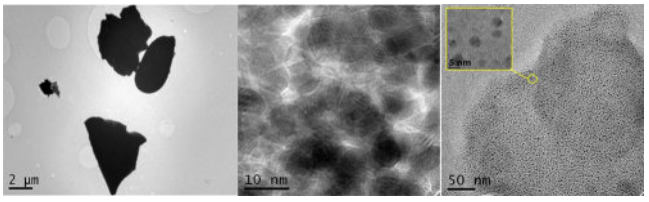

Figure 2. HR-TEM images of (a) micron Cu_2O, (b) nano Cu_2O, and (c) Ag/Cu_2O. (The inset shows magnified Ag nanoparticles of ~5 nm surrounded by Cu_2O. Scale of insert is 5 nm.)

Cu_2O (Figure 4). To obtain the band gap data, DRS was used, and corresponding absorbance plot and subsequent conversion to Kubelka–Munk plot are shown in Figure 3. From DRS, it was determined that the band gap energies for Cu_2O micron size and Cu_2O nanosize were 1.9 and 2.3 eV, respectively. Cyclic voltammetry was used to place band gap values on an absolute NHE scale. It was found that nanosized Cu_2O has a slightly larger band gap than micron-sized Cu_2O due to quantum confinement[47] (Table 1; Supporting Information, Figure S6). Since a Ag/AgCl reference electrode was used, eq 3 is used to convert to normal hydrogen electrode (NHE) values.[48]

$$E(\text{NHE}) = E(\text{Ag/AgCl}) + 0.197 \text{ V} \quad (3)$$

With the particles fully characterized, photoexperiments were conducted to test for formate production. Based on previous studies, it was found that formate production is pH-dependent. At a pH of 8.5, HCO_3^- is the predominant species present, and is therefore expected to be the species undergoing reduction.[10]

Table 2 and Table S1 (Supporting Information) show the boost in formate production under air mass coefficient 0 (AM 0) as opposed to air mass coefficient 1.5 (AM 1.5) solar simulation irradiation. Metal oxide semiconductors are primarily photoexcited by UV radiation, but the AM 1.5 filter blocks much of the higher-frequency UV radiation between 300 and 400 nm. Under both AM 1.5 and AM 0 conditions, nanoparticulate Cu_2O yielded a higher formate production than micron-sized Cu_2O (Figure 8; Supporting Information, Figure S8), with respective productivities of 0.76 and 0.37 mmol formate/(g_{cat} h) in IPA, and 1.99 and 0.93 mmol formate/(g_{cat} h) in glycerol (Figure 8, Table 2; Supporting Information, Table S1). To the best of our knowledge, these are the highest production levels reported for CO_2 conversion to formate using Cu_2O as a photocatalyst. With $(Cu_2O)^*$ as the photoexcited semiconductor, the proposed redox mechanism of Cu_2O semiconductor photocatalysis is shown in Figure 5a and Scheme 1. After photoexcitation and the generation of electrons and holes, subsequent reduction of HCO_3^- to HCO_3^{2-} and finally to HCO_2^- takes place. The other half reaction takes place when 2-propanol scavenges photogenerated holes and undergoes oxidation to acetone. For confirmation of the reaction mechanism in Figure 5, acetone was detected and quantified by a gas chromatograph (GC). A linear increase of acetone was observed between 0 and 8 h (Supporting Information, Figure S7).

Studies have shown that plasmon-excited nanoparticles can create hot electrons with energies between the vacuum level and the work function of the metal.[49] These hot electrons arise from plasmon decay and, in this transient state, can transfer charge into other species to catalyze chemical reactions. With AgNPs we observe formate production comparable to that of a semiconductor (Figure 9), with respective productivities of

DOI: 10.1021/acssuschemeng.7b03244
ACS Sustainable Chem. Eng. 2018, 6, 1872–1880

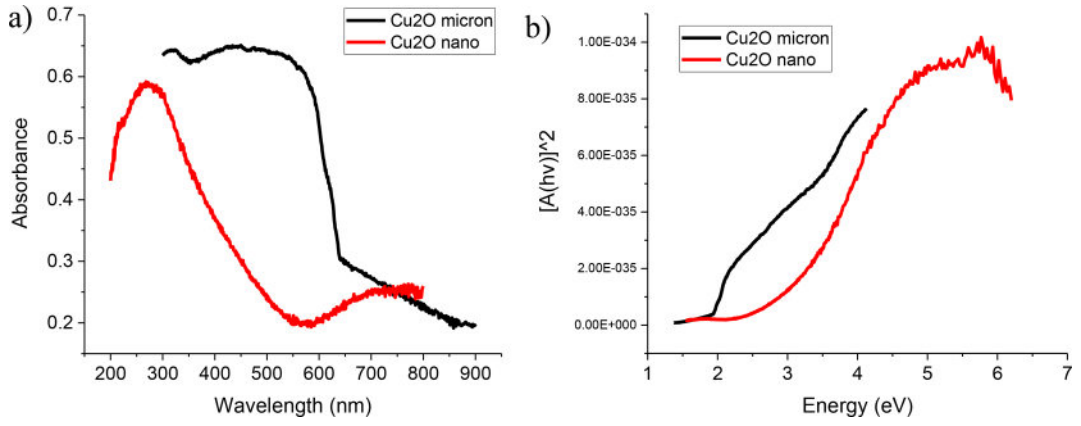

Figure 3. (a) Diffuse reflectance spectroscopy of Cu_2O micron- and nanosize absorbance. (b) Kubelka–Munk treated plot.

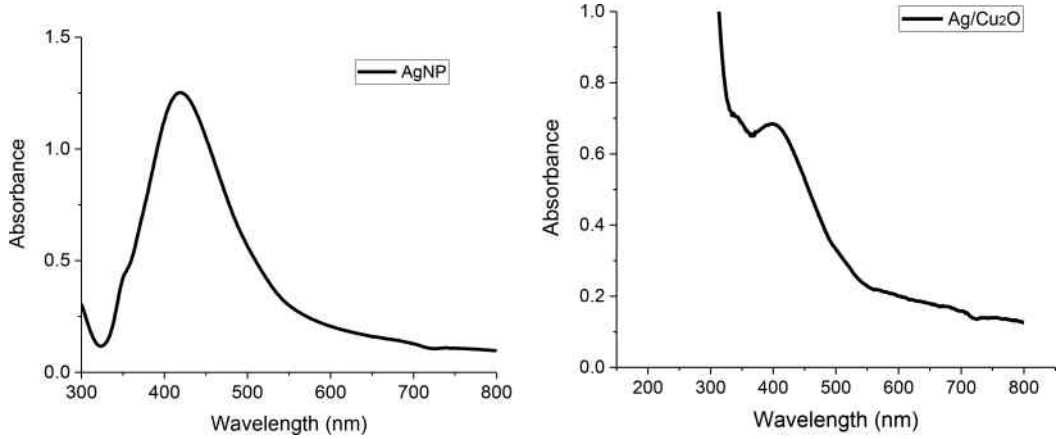

Figure 4. UV–vis spectra of silver nanoparticles (AgNPs; left) and nanocomposite Ag/Cu_2O (right).

Table 1. Valence Band, Conduction Band, and Band Gap Values[a] for Cu_2O

	Cu_2O (eV)	
	literature[18]	experimental
VB	1.3	1.067 (nano)
	1.3	1.01 (micron)
CB	−0.7	−0.89 (nano)
	−0.7	−0.87 (micron)
band gap	2.0	1.96 (nano)
	2.0	1.88 (micron)

[a]Experimental values are obtained from cyclic voltammetry.

Table 2. Productivity [mmol Formate/(g_{cat} h)] of Cu_2O, AgNP, and Ag/Cu_2O in IPA and Glycerol[a]

particle population	productivity in IPA AM 1.5	productivity in glycerol AM 1.5
Cu_2O micron	0.067 ± 0.007	0.47 ± 0.008
Cu_2O nano	0.37 ± 0.02	0.93 ± 0.04
Ag/Cu_2O	0.066 ± 0.0007	2.76 ± 0.1
Ag	0.053 ± 0.0002	0.75 ± 0.03

[a]All reported values are from triplicate measurements.

0.053 mmol formate/(g_{cat} h) in IPA and 0.75 mmol formate/(g_{cat} h) in glycerol (Table 2). Ag/Cu_2O showed the highest productivity in glycerol of 2.76 (AM 1.5) and 3.41 (AM 0) mmol formate/(g_{cat} h) (Figure 10, Table 2; Supporting Information, Table S1). In IPA, this nanocomposite catalyst had much lower productivity of 0.066 (AM 1.5) and 0.091 (AM 0) mmol formate/(g_{cat} h) (Table 2; Supporting Information, Table S1).

AgNPs have been shown to enhance photocatalysis because these nanoparticles scavenge $^{\bullet}OH$ radicals.[50] The scavenging of $^{\bullet}OH$ radicals is expected to increase formate production because $^{\bullet}OH$ radicals are detrimental to formate production. $^{\bullet}OH$ radicals can react with both bicarbonate and formate, hence the deleterious effect on overall formate production (eqs 4–6).[51] Since previous experiments have used plasmonic metallic nanoparticles as a sensitizer for TiO_2 and have successfully demonstrated electron and resonant energy transfer from nanoparticles to semiconductor,[52−54] we attempted to apply AgNPs as a sensitizer for Cu_2O.

$$HCO_3^- + 2e^- + 2H^+ \rightarrow HCO_2^- + H_2O \quad (4)$$

$$HCO_3^- + OH^{\bullet} \rightarrow CO_3^{\bullet -} + H_2O \quad (5)$$

$$OH^{\bullet} + HCO_2^- \rightarrow H_2O + CO_2^{\bullet -} \quad (6)$$

In a control experiment, silver nanoparticles added to Cu_2O (i.e., Ag Cu_2O) showed no enhancement in formate production (Supporting Information, Figure S9), with productivity of 0.37 mmol formate/(g_{cat} h) when added to micron Cu_2O and 0.56 mmol formate/(g_{cat} h) when added to nanoparticulate Cu_2O in glycerol. This observation is expected due to the incompatibility of the VB and CB energies of Cu_2O and the Fermi level of silver nanoparticles. Since the valence band and conduction band energies for Cu_2O do not allow for the generation of $^{\bullet}OH$

DOI: 10.1021/acssuschemeng.7b03244
ACS Sustainable Chem. Eng. 2018, 6, 1872−1880

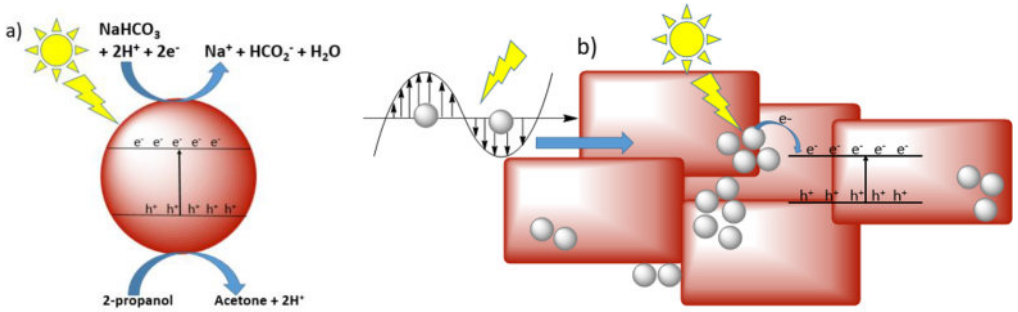

Figure 5. Proposed mechanism for (a) Cu_2O semiconductor and (b) Ag/Cu_2O. (Blue block arrow represents resonant energy transfer from metal to semiconductor.)

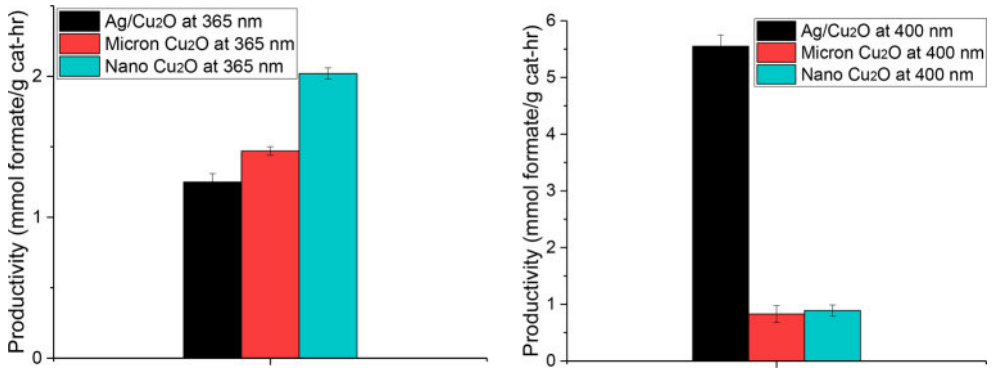

Figure 6. Formate productivity from select wavelength experiments at (left) 365 and (right) 400 nm.

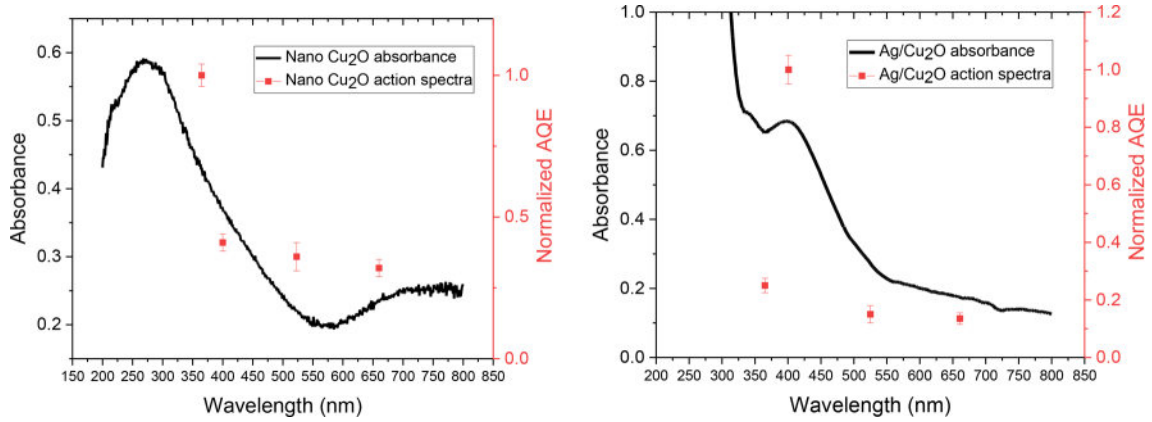

Figure 7. Action spectra of (left) nano Cu_2O and (right) Ag/Cu_2O.

radicals, adding AgNP to Cu_2O does not increase formate production.

Interestingly, the nanocomposite Ag/Cu_2O system shows significant enhancement of formate production. Within a nanocomposite system, there are different mechanisms in which the plasmonic metal can enhance the performance of the semiconductor. The photoexcited plasmons in the metal can decay radiatively re-emitting photons and concentrate electromagnetic field at the molecular scale. Surface plasmons at the metal can also relax nonradiatively creating a transient population of nonequilibrium (hot) charge carriers or by releasing thermal energy. The hot electrons can be transferred to the conduction band of the semiconductor. The localization of electromagnetic fields close to the metal−semiconductor interface and the enhanced supply of electrons to semiconductor conduction band can improve the overall photocatalytic efficiency of the system. Figure 5b illustrates both direct electron transfer and plasmon energy transfer from metal (represented by silver spheres) to semiconductor (represented by red rectangles); both are responsible for the enhanced performance of the semiconductor through LSPR-induced charge separation in the semiconductor.

Control experiments were performed under dark conditions for 8 h for both Cu_2O and Ag/Cu_2O nanocomposites (Supporting Information, Figure S10). In both cases the production of formate was negligible confirming the importance of their photocatalytic effect. For confirmation of the plasmonic effect of silver, wavelength-dependent experiments were performed at four select wavelengths of 365, 400, 525, and 660 nm for micron Cu_2O, nano Cu_2O, and Ag/Cu_2O composites. The wavelength of 365 nm is the absorption maximum for Cu_2O, but the plasmonic effect of silver is not very pronounced at this wavelength. As expected, at this wavelength an increase in formate production is observed with

DOI: 10.1021/acssuschemeng.7b03244
ACS Sustainable Chem. Eng. 2018, 6, 1872−1880

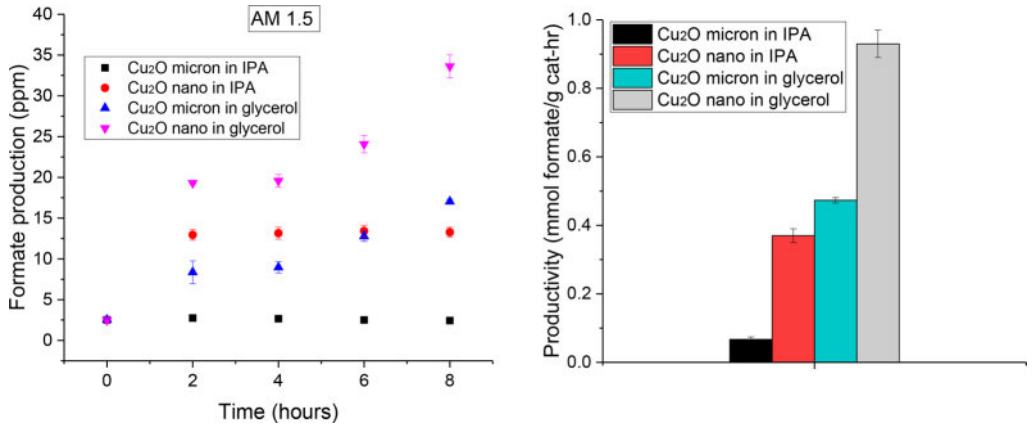

Figure 8. (left) Formate production (in ppm) and (right) productivity with micron and nanoparticulate Cu_2O in IPA and glycerol under AM 1.5 irradiation.

Scheme 1. Proposed Mechanism for the Conversion of Bicarbonate to Formate

Illumination:

$$Cu_2O \xrightarrow{h\nu} Cu_2O^*(h^+ + e^-)$$

Oxidation:

$$(CH_3)_2CHOH \xrightarrow[(Cu_2O)^*]{h^+} 2H^+ + (CH_3)_2CO$$

Reduction:

$$HCO_3^- \xrightarrow[(Cu_2O)^*]{e^-} HCO_3^{2-}$$

$$HCO_3^{2-} \xrightarrow[(Cu_2O)^*]{2H^+ + e^-} HCO_2^- + H_2O$$

both micron and nano Cu_2O, and minimal enhancement with Ag/Cu_2O is observed (Figure 6, left). Near the plasmonic peak of Ag nanoparticles at 400 nm, a significant enhancement in the production of formate is observed with Ag/Cu_2O composites (Figure 6, right), which is attributed to the plasmonic effect of Ag nanoparticles. At the 400 nm wavelength the absorbance of Cu_2O is negligible; the observed improvement cannot be solely explained by increased light absorption on Cu_2O due to plasmon-induced resonance energy transfer from Ag to Cu_2O. Plasmonic heating cannot be the main reason for the observed enhancement effect either, since CO_2 to formate requires the energy of 0.61 V, which is higher than the thermal energy generated by plasmonic heating under solar irradiation.[7,55] The Fermi level of Ag is −4.2 eV,[56] with an interband transition of 3.8 eV (~330 nm).[57] The energy gap between the conduction band of Cu_2O and the Fermi level of Ag is 1.1 eV. Any light absorbed above 330 nm is expected to promote electrons from the Fermi level of Ag nanoparticles to the conduction band of Cu_2O. Hence, the plasmon-induced hot electron transfer from silver nanoparticles to Cu_2O seems to play the most important role here. These effects are further confirmed by the action spectra (Figure 7), which study the wavelength dependency of AQE. The AQE is highest at the absorption maximum of Cu_2O and plasmonic peak of silver nanoparticles.

Bicarbonate reduction requires a sacrificial agent to fill photogenerated holes, thus reducing charge recombination. As a control experiment, the photocatalytic reaction with Ag was carried out without a hole scavenger, and very low amounts of formate were produced (Supporting Information, Figure S11). Based on earlier work including our own, 2-propanol and glycerol were chosen because they both contain secondary donor hydrides. Glycerol possesses one secondary and two primary alcohol groups available for oxidation, whereas 2-propanol only has one secondary alcohol group. Among the positive hole scavengers compared in this study, 2-propanol is derived from petroleum sources. Glycerol, on the other hand, is

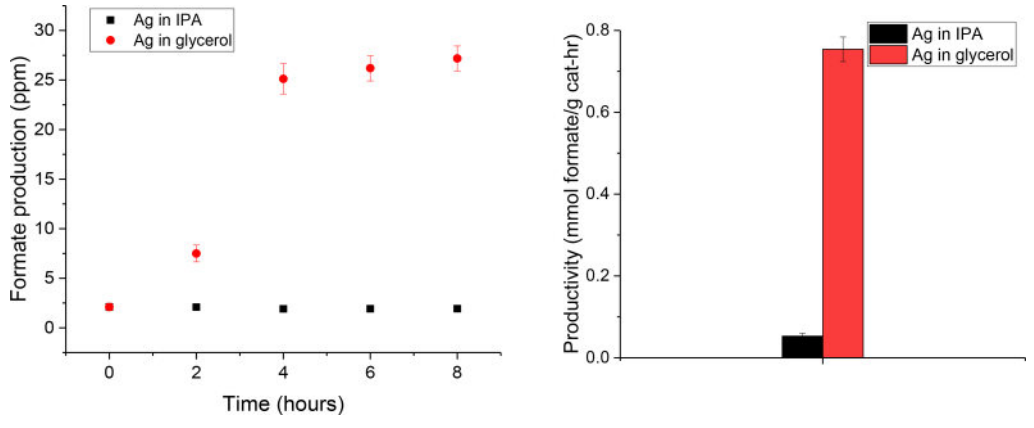

Figure 9. (left) Formate production and (right) productivity with AgNP only, without Cu_2O.

DOI: 10.1021/acssuschemeng.7b03244
ACS Sustainable Chem. Eng. 2018, 6, 1872−1880

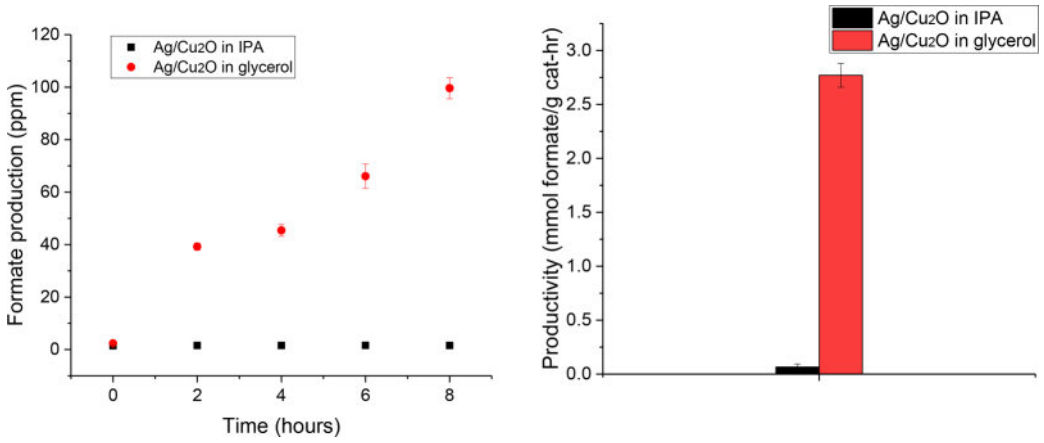

Figure 10. (left) Formate production and (right) productivity with Ag/Cu_2O nanocomposite in IPA and glycerol under AM 1.5 conditions.

Table 3. Summary of Semiconductor Characterization[a]

particle population	crystal type	diameter (nm)	surface area (m^2/g)	AQE in IPA (%) AM 1.5	AQE in glycerol (%) AM 1.5
Cu_2O micron	cubic	<5000	1.27 ± 0.6	0.14 ± 0.01	0.95 ± 0.02
Cu_2O nano	cubic	<350	6.48 ± 1.1	0.74 ± 0.03	1.87 ± 0.08
Ag/Cu_2O	—[b]	all ~5000 ± 15	—	0.13 ± 0.002	5.53 ± 0.2
AgNP	—	12.89 ± 1.5	—	0.106 ± 0.0005	1.51 ± 0.07

[a]All reported values are from triplicate measurements. [b]—, measurement was not performed (Ag/Cu_2O and AgNP samples were in aqueous solution, and thus the crystal structure and surface area could not be determined by the instrument).

of interest because it derives from plants, is low-cost, environmentally benign, and relatively abundant. It has been shown in this work, as well as in that of Leonard et al., that glycerol is a more efficient hole scavenger than IPA. This feature derives from the number of available primary hydrides and secondary hydroxyl carbons available in glycerol.[10] Coupled with these more recent results, use of glycerol is expected to be a far superior hole scavenger than IPA.

Formate production can be quantified in terms of apparent quantum efficiency (AQE), calculated by eqs 1 and 2. Table 3 and Table S1 (Supporting Information) summarize the different forms of Cu_2O tested. Possessing greater surface area, nanoparticulate Cu_2O yielded a higher AQE than micron-sized Cu_2O. Under AM 1.5 conditions, micron-sized Cu_2O generated an AQE of 0.14% in IPA and 0.95% in glycerol; and 0.15% and 3.65% in IPA and glycerol under AM 0 conditions. Nanoparticulate Cu_2O yielded an AQE of 0.74% in IPA and 1.87% in glycerol under AM 1.5 conditions; and 1.52% and 3.99% under AM 0 conditions. AgNP alone was able to produce an AQE of 0.11% in IPA and 1.51% in glycerol. Ag/Cu_2O in glycerol showed the highest AQE of 5.53% (AM 1.5) and 6.82% (AM 0).

CONCLUSION

In summary, a new set of nontoxic and Earth-abundant semiconductor materials have shown photochemical efficacy in the conversion of bicarbonate to formate. Micron and nanoparticulate Cu_2O, nanocomposite Ag/Cu_2O, and silver nanoparticles added to Cu_2O were characterized and examined for their photochemical properties. Because of its higher surface area and smaller band gap, as expected, nanoparticulate Cu_2O proved to be a more efficient photocatalyst than micron-sized Cu_2O. Although silver NPs have been shown to scavenge $^{\bullet}OH$ radicals, a species deleterious to the bicarbonate/formate conversion, we observed no enhancement in formate production upon the inclusion of AgNP with Cu_2O. These findings confirm the favorable VB/CB energy levels of Cu_2O, with regard to their suitability for electron transfer to bicarbonate, but no other reactant or solvent species. Significantly enhanced formate production is apparent with Ag/Cu_2O due to plasmon-induced electron transfer from Ag to Cu_2O. The recent developments in nanocomposite architectures such as Ag/Cu_2O have found an important application here via plasmonic properties of metallic nanoparticles that harness resonant energy to enhance semiconductor efficiency. This study reports the highest quantum efficiency values compared to previous CO_2 or bicarbonate to formate conversions. Future studies include the use of other semiconductors, with similar nanocomposite systems, and the use of ultrafast spectroscopy to further elucidate charge carrier dynamics and the reaction mechanism of plasmon-enhanced photocatalysis.

ASSOCIATED CONTENT

Supporting Information

The Supporting Information is available free of charge on the ACS Publications website at DOI: 10.1021/acssuschemeng.7b03244.

Rate vs photocatalyst concentration, XRD spectra, DLS size distribution, EDS results, UV−vis spectra, CV curve, acetone production vs time, formate production vs time, and productivity and AQE values (PDF)

AUTHOR INFORMATION

Corresponding Author

*E-mail: michael.heagy@nmt.edu.

ORCID

Sanchari Chowdhury: 0000-0002-9875-1026

Michael D. Heagy: 0000-0002-4519-078X

DOI: 10.1021/acssuschemeng.7b03244
ACS Sustainable Chem. Eng. 2018, 6, 1872−1880

Notes

The authors declare no competing financial interest.

■ ACKNOWLEDGMENTS

The authors gratefully acknowledge NSF award # IIA-1301346 for financial support. S.O. thanks the NSF EPSCoR STEMAP program for summer research support.

■ REFERENCES

(1) Olah, G. A.; Goeppert, A.; Prakash, G. K. S. Chemical Recycling of Carbon Dioxide to Methanol and Dimethyl Ether: From Greenhouse Gas to Renewable, Environmentally Carbon Neutral Fuels and Synthetic Hydrocarbons. *J. Org. Chem.* **2009**, *74*, 487−498.

(2) Olah, G. A.; Prakash, G. K. S.; Goeppert, A. Anthropogenic Chemical Carbon Cycle for a Sustainable Future. *J. Am. Chem. Soc.* **2011**, *133*, 12881−12898.

(3) Halmann, M. M. *Meyer Steinberg. Greenhouse Gas Carbon Dioxide Mitigation: Science and Technology*; CRC Press LLC, Lewis Publishers, 1999.

(4) White, J. L.; Herb, J. T.; Kaczur, J. J.; Majsztrik, P. W.; Bocarsly, A. B. Photons to Formate: Efficient Electrochemical Solar Energy Conversion Via Reduction of Carbon Dioxide. *Journal of CO2 Utilization* **2014**, *7*, 1−5.

(5) Olah, G. A.; Goeppert, A.; Surya Prakash, G. K. *Beyond Oil and Gas: The Methanol Economy*, 2nd ed.; Wiley-VCH, 2011.

(6) John, R.; Florence, S. Optical, structural and morphological studies of bean-like ZnS nanostructures by aqueous chemical method. *Chalcogenide Lett.* **2010**, *7* (4), 269−273.

(7) Habisreutinger, S. N.; Schmidt-Mende, L.; Stolarczyk, J. K. Photocatalytic Reduction of CO_2 on TiO_2 and Other Semiconductors. *Angew. Chem., Int. Ed.* **2013**, *52*, 7372−7408.

(8) Henglein, A.; Gutierrez, M.; Fischer, C. H. Photochemistry of Colloidal Metal Sulfides 6. Kinetics of Interfacial Reactions at ZnS-Particles. *Ber. Bunsenges. Phys. Chem.* **1984**, *88*, 170−175.

(9) Yoneyama, H. Photoreduction of Carbon Dioxide on Quantized Semiconductor Nanoparticles in Solution. *Catal. Today* **1997**, *39*, 169−175.

(10) Leonard, D. P.; Pan, H.; Heagy, M. D. Photocatalzyed Reduction of Bicarbonate to Formate: Effect of ZnS Crystal Structure and Positive Hole Scavenger. *ACS Appl. Mater. Interfaces* **2015**, *7*, 24543−24549.

(11) Johne, P.; Kisch, H. Photoreduction of Carbon Dioxide Catalysed by Free and Supported Zinc and Cadmium Sulphide Powders. *J. Photochem. Photobiol., A* **1997**, *111*, 223−228.

(12) Kanemoto, M.; Shiragami, T.; Pac, C.; Yanagida, S. Semiconductor Photocatalysis. Effective Photoreduction of Carbion Dioxide Catalyzed by ZnS Quantum Crystallites with Low Density of Surface Defects. *J. Phys. Chem.* **1992**, *96*, 3521−3526.

(13) Inoue, H.; Moriwaki, H.; Maeda, K.; Yoneyama, H. Photoreduction of Carbon Dioxide Using Chalcogenide Semiconductor Microcrystals. *J. Photochem. Photobiol., A* **1995**, *86*, 191−196.

(14) Kuwabata, S.; Nishida, K.; Tsuda, R.; Inoue, H.; Yoneyama, H. Photochemical Reduction of Carbon Dioxide to Methanol Using ZnS Microcrystallite as Photocatalyst in the Presence of Methanol Dehydrogenase. *J. Electrochem. Soc.* **1994**, *141*, 1498−1503.

(15) Kaneco, S.; Kurimoto, H.; Ohta, K.; Mizuno, T.; Saji, A. Photocatalytic Reduction of CO_2 Using TiO_2 powders in Liquid CO_2 Medium. *J. Photochem. Photobiol., A* **1997**, *109*, 59−63.

(16) Kaneco, S.; Shimizu, Y.; Ohta, K.; Mizuno, T. Photocatalytic Reduction of High Pressure Carbon Dioxide Using TiO_2 Powders with a Positive Hole Savenger. *J. Photochem. Photobiol., A* **1998**, *115*, 223−226.

(17) Yu, J.; Low, J.; Xiao, W.; Zhou, P.; Jaroniec, M. Enhanced Photocatalytic CO_2-Reduction Activity of Anatase TiO_2 by Coexposed {001} and {101} facets. *J. Am. Chem. Soc.* **2014**, *136*, 8839−8842.

(18) Liu, X.; Inagaki, S.; Gong, J. Heterogeneous Molecular Systems for Photocatalytic CO_2 Reduction with Water Oxidation. *Angew. Chem., Int. Ed.* **2016**, *55*, 14924−14950.

(19) Chang, X.; Wang, T.; Gong, J. CO_2 Photo-reduction: Insights into CO_2 Activation and Reaction on Surfaces of Photocatalysts. *Energy Environ. Sci.* **2016**, *9*, 2177−2196.

(20) Yin, G.; Nishikawa, M.; Nosaka, Y.; Srinivasan, N.; Atarashi, D.; Sakai, E.; Miyauchi, M. Photocatalytic Carbon Dioxide Reduction by Copper Oxide Nanocluster-Grafted Niobate Nanosheets. *ACS Nano* **2015**, *9*, 2111−2119.

(21) Tennakone, K.; Jayatissa, A. H.; Punchihewa, S. Selective Photoreduction of Carbon Dioxide to Methanol with Hydrous Cuprous Oxide. *J. Photochem. Photobiol., A* **1989**, *49*, 369−375.

(22) Li, H.; Lei, Y.; Huang, Y.; Fang, Y.; Xu, Y.; Zhu, L.; Li, X. Photocatalytic Reduction of Carbion Dioxide to Methanol by Cu_2O/SiC Nanocrystallite Under Visible Light Irradiation. *J. Nat. Gas Chem.* **2011**, *20*, 145−150.

(23) Janaky, C.; Hursan, D.; Endrodi, B.; Chanmanee, W.; Roy, D.; Liu, D.; de Tacconi, N. R.; Dennis, B. H.; Rajeshwar, K. Electro- and Photoreduction of Carbon Dioxide: The Twain Shall Meet at Copper Oxide/Copper Interfaces. *ACS Energy Lett.* **2016**, *1*, 332−338.

(24) Li, C. W.; Kanan, M. W. CO_2 Reduction at Low Overpotential on Cu Electrodes Resulting from the Reduction of Thick Cu_2O Films. *J. Am. Chem. Soc.* **2012**, *134*, 7231−7234.

(25) Kas, R.; Kortlever, R.; Milbrat, A.; Koper, M. T. M.; Mui, G.; Baltrusaitis, J. Electrochemical CO_2 Reduction on Cu_2O-derived Copper Nanoparticles: Controlling the Catalytic Selectivity of Hydrocarbons. *Phys. Chem. Chem. Phys.* **2014**, *16*, 12194−12201.

(26) Le, M.; Ren, M.; Zhang, Z.; Sprunger, P. T.; Kurtz, R. L.; Flake, J. C. Electrochemical Reduction of CO_2 to CH_3OH at Copper Oxide Surfaces. *J. Electrochem. Soc.* **2011**, *158* (5), E45−E49.

(27) Chang, X.; Wang, T.; Zhang, P.; Wei, Y.; Zhao, J.; Gong, J. Stable Aqueous Photoelectrochemical CO_2 Reduction by a Cu_2O Dark Cathode with Improved Selectivity for Carbonaceous Products. *Angew. Chem., Int. Ed.* **2016**, *55*, 8840−8845.

(28) Paracchino, A.; Brauer, J. C.; Moser, J.-E.; Thimsen, E.; Graetzel, M. Synthesis and Characterization of High-Photoactivity Electrodeposited Cu_2O Solar Absorber by Photoelectrochemistry and Ultrafast Spectroscopy. *J. Phys. Chem. C* **2012**, *116*, 7341−7350.

(29) Ghadimkhani, G.; de Tacconi, N. R.; Chanmanee, W.; Janaky, C.; Rajeshwar, K. Efficient Solar Photoelectrosynthesis of Methanol from Carbon Dioxide Using Hybrid CuO-Cu_2O Semiconductor Nanorod Arrays. *Chem. Commun.* **2013**, *49*, 1297−1299.

(30) Lee, S.; Park, G.; Lee, J. Importance of Ag-Cu Biphasic Boundaries for Selective Electrochemical Reduction of CO_2 to Ethanol. *ACS Catal.* **2017**, *7*, 8594−8604.

(31) Chen, S.; Wang, L.-W. Thermodynamic Oxidation and Reduction Potentials of Photocatalytic Semiconductors in Aqueous Solution. *Chem. Mater.* **2012**, *24*, 3659−3666.

(32) Colmenares, J. C.; Aramendia, M. A.; Marinas, A.; Marinas, J. M.; Urbano, F. J. Synthesis, Characterization and Photocatalytic Activity of Different Metal-doped Titania Systems. *Appl. Catal., A* **2006**, *306*, 120−127.

(33) Koci, K.; Mateju, K.; Obalova, L.; Krejcikova, S.; Lacny, Z.; Placha, D.; Capek, L. Effect of Silver Doping on the TiO_2 for Photocatalytic reduction of CO_2. *Appl. Catal., B* **2010**, *96*, 239−244.

(34) Krejcikova, S.; Matejova, L.; Koci, K.; Obalova, L.; Matej, Z.; Capek, L.; Solcova, O. Preparation and Characterization of Ag-doped Crystalline Titania for Photocatalysis Applications. *Appl. Catal., B* **2012**, *111*, 119−125.

(35) Kooij, E. S.; Ahmed, W.; Zandvliet, H. J. W.; Poelsema, B. Localized Plasmons in Noble Metal Nanospheroids. *J. Phys. Chem. C* **2011**, *115*, 10321−10332.

(36) Zhang, X.; Zhang, J.; Wang, H.; Hao, Y.; Zhang, X.; Wang, T.; Wang, Y.; Zhao, R.; Zhang, H.; Yang, B. Thermal-induced surface plasmon band shift of gold nanoparticle monolayer: morphology and refractive index sensitivity. *Nanotechnology* **2010**, *21*, 465702-1−465702-11.

(37) Linic, S.; Christopher, P.; Xin, H.; Marimuthu, A. Catalytic and Photocatalytic Transformations on Metal Nanoparticles with Targeted Geometric and Plasmonic Properties. *Acc. Chem. Res.* **2013**, *46*, 1890−1899.

DOI: 10.1021/acssuschemeng.7b03244
ACS Sustainable Chem. Eng. 2018, 6, 1872−1880

(38) Zhang, X.; Chen, Y. L.; Liu, R.-S.; Tsai, D. P. Plasmonic Photocatalysis. *Rep. Prog. Phys.* **2013**, *76*, 046401.
(39) Liu, E.; Kang, L.; Wu, F.; Sun, T.; Hu, X.; Yang, Y.; Liu, H.; Fan, J. Photocatalytic Reduction of CO_2 into Methanol over Ag/TiO_2 Nanocomposites Enhanced by Surface Plasmon Resonance. *Plasmonics* **2014**, *9*, 61−70.
(40) Li, J.; Cushing, S. K.; Bright, J.; Meng, F.; Senty, T. R.; Zheng, P.; Bristow, A. D.; Wu, N. $Ag@Cu_2O$ Core-Shell Nanoparticles as Visible-Light Plasmonic Photocatalysts. *ACS Catal.* **2013**, *3*, 47−51.
(41) Ledwith, D. M.; Whelan, A. M.; Kelly, J. M. A Rapid, Straight-Forward Method for Controlling the Morphology of Stable Silver Nanoparticles. *J. Mater. Chem.* **2007**, *17*, 2459−2464.
(42) Fang, Y. M.; Sun, J. J.; Wu, A. H.; Su, X. L.; Chen, G. N. Catalytic Electrogenerated Chemiluminescence and Nitrate Reduction at CdS Nanotubes Modified Glassy Carbon Electrode. *Langmuir* **2009**, *25*, 555−560.
(43) Kisch, H.; Bahnemann, D. Comparing Rates or Apparent Quantum Yields? *J. Phys. Chem. Lett.* **2015**, *6*, 1907−1910.
(44) Lewis, N.; Nocera, D. Powering the Planet: Chemical Challenges in Solar Energy Utilization. *Proc. Natl. Acad. Sci. U. S. A.* **2006**, *103*, 15729−15735.
(45) Quigg, A.; Chin, W. C.; Chen, C. S.; Zhang, S. J.; Jiang, Y. L.; Miao, A.; Schwehr, K. A.; Xu, C.; Santschi, P. Direct and Indirect Toxic Effects of Engineered Nanoparticles on Algae: Role of Natural Organic Matter. *ACS Sustainable Chem. Eng.* **2013**, *1*, 686−702.
(46) Klabunde, K. J.; Richards, R. M. *Nanoscale Materials in Chemistry*, 2nd ed.; John Wiley & Sons, Inc.: Hoboken, NJ, 2009.
(47) Alivisatos, A. P. Semiconductor Clusters, Nanocrystals, and Quantum Dots. *Science* **1996**, *271*, 933−937.
(48) Bard, A. J.; Faulkner, L. R. *Electrochemical Methods: Fundamentals and Applications*; John Wiley & Sons: New York, 2000.
(49) Mukherjee, S.; Libisch, F.; Large, N.; Neumann, O.; Brown, L. V.; Cheng, J.; Lassiter, J. B.; Carter, E. A.; Nordlander, P.; Halas, N. J. Hot Electrons Do the Impossible: Plasmon-Induced Dissociation of H_2 on Au. *Nano Lett.* **2013**, *13*, 240−247.
(50) He, D.; Jones, A. M.; Garg, S.; Pham, A. N.; Waite, T. D. Silver Nanoparticle-Reactive Oxygen Species Interactions: Applications of a Charging-Discharging Model. *J. Phys. Chem. C* **2011**, *115*, 5461−5468.
(51) Molinari, A.; Samiolo, L.; Amadelli, R. EPR Spin Trapping Evidence of Radical Intermediate in the Photo-reduction of Bicarbonate/CO_2 in TiO_2 aqueous Suspensions. *Photochem. Photobiol. Sci.* **2015**, *14*, 1039−1046.
(52) Ide, Y.; Matsuoka, M.; Ogawa, M. Efficient Visible-Light-Induced Photocatalytic Activity on Gold-Nanoparticle-Supported Layered Titanate. *J. Am. Chem. Soc.* **2010**, *132*, 16762−16764.
(53) Christopher, P.; Ingram, D. B.; Linic, S. Enhncing Photochemical Activity of Semiconductor Nanoparticles with Optically Active Ag Nanostructures: Photochemistry Mediated by Ag Surface Plasmons. *J. Phys. Chem. C* **2010**, *114*, 9173−9177.
(54) Ingram, D. B.; Linic, S. Water Splitting on Composite Plasmonic-Metal/Semiconductor Photoelectrodes: Evidence for Selective Plasmon-Induced Formation of Charge Carriers near the Semiconductor Surface. *J. Am. Chem. Soc.* **2011**, *133*, 5202−5205.
(55) Sarina, S.; Jaatinen, E.; Xiao, Q.; Huang, Y. M.; Christopher, P.; Zhao, J. C.; Zhu, H. Y. Photon Energy Threshold in Direct Photocatalysis with Metal Nanoparticles: Key Evidence from the Action Spectrum of the Reaction. *J. Phys. Chem. Lett.* **2017**, *8*, 2526−2534.
(56) *CRC Handbook of Chemistry and Physics*; Lide, D. R., Ed.; CRC Press, 2008.
(57) Johnson, P.; Christy, R. Optical Constants of the Noble Metals. *Phys. Rev. B: Solid State* **1972**, *6*, 4370.

DOI: 10.1021/acssuschemeng.7b03244
ACS Sustainable Chem. Eng. 2018, 6, 1872−1880

CONSPECTUS

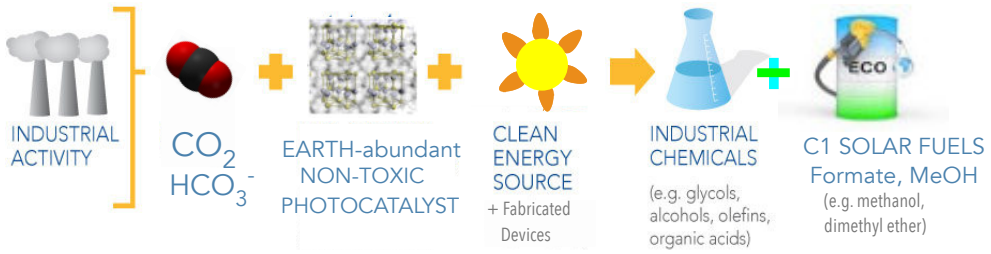

Since CO_2 can be recovered from a variety of industrial sources and exists in its neutral hydrated form as bicarbonate, the current unabated production of this greenhouse gas makes it a potential feedstock for regeneration via solar fuels. As a potential negative emission technology (NET), the chemical conversion of carbon dioxide and/or bicarbonate to C-1 products such as formate or methanol underscores a second advantage, mainly economic as this greenhouse gas becomes value-added in comparison to being sequestered. As a chemical feedstock, formate or depending on pH, methanoic acid functions in a number of industrial, medical and agricultural applications ranging from preservative, food additive, and antibacterial agent in livestock feed. Methanoic acid can be converted to methanol as a high-octane number end product. This concept of the "methanol economy", has been highlighted as an alternative to hydrogen fuel because methanol is regenerative via CO_2 and more readily transportable.

International Solar Fuels Conference, San Diego CA, July 6-10, 2017
NMT's Hanqing Pan with Dr. Daniel G. Nocera - Patterson Rockwood Professor of Energy
Harvard University, Chemistry Dept. *Time* magazine 100 most influential people; h-index 85

In Hanqing Pan's research, new nanostructures along with their respective chemical components comprise much of her research endeavors. The first aspect involves new fabrication techniques resulting in nanoparticles, nanosheets, nanotubes, nanorods, nanobelts, and nanoflowers with the express intent to afford high specific surface areas. Another parameter, the chemical component, involves optimization of the semiconductor band gap with improvements in metal oxides, metal sulfides, multicomponent oxides, or doping with metal ions, anions or trace amounts noble metals. An additional challenge for consideration of any photocatalyst concerns the matter of utilizing non-toxic and earth-abundant materials toward solar fuel development. Her outstanding scientific research paper in *ACS Sustainable Chemistry and Engineering;* Impact Factor 5.95 (2015) presents a number of sustainable chemistry findings regarding reduction/oxidation chemistry combined with nanotechnology and one-sun input. Although appearing in print in February 2018, the article was published on the web as an *ACS/ASAP* in Dec 07, 2017. If this timeline is unacceptable to the committee, an added and earlier paper by Ms. Pan appearing in November 2017 is attached as well.